A NEW ROTATING TEST FACILITY FOR THE EXPERIMENTAL CHARACTERISATION OF SHAFT SEALS

E Pedraza-Valle[1], JA Scobie[1], CM Sangan[1], PS Keogh[1], A Bowsher[2] and PF Crudgington[2]

[1]Department of Mechanical Engineering, University of Bath, United Kingdom, BA2 7AY

[2]Cross Manufacturing Co. (1938) Ltd, Devizes, United Kingdom, SN10 2EU

ABSTRACT

Turbomachinery shaft seals suffer from rubs caused by thermal growth, assembly misalignment and rotor dynamic vibration at engine start-up and shut-down. Rubs are detrimental to performance, leading to a decrease in overall efficiency and costly corrective maintenance. In recent years, compliant seals have been developed, allowing for variable clearances and a reduced frequency of seal rubs. The design goal for compliant seals is therefore, to maintain a tight clearance between rotating and non-rotating parts, throughout the transient conditions experienced in engines.

This paper presents the design of a new high-speed rotating test facility developed for the performance characterisation of turbine shaft seals. The rig features a 254 mm diameter rotor, capable of rotating at speeds of up to 15,000 rpm (equivalent to rotor surface speeds up to 200 m/s). The maximum pressure difference across a seal is 3.5 bar.

In the first experimental campaign, the performance of a labyrinth seal was investigated. The rotordynamic coefficients of the seal were calculated by exciting the casing with an electromagnetic shaker. The leakage performance, direct and cross-coupled seal stiffnesses and effective damping coefficients are determined.

KEY WORDS

LABYRINTH SEALS, ROTORDYNAMICS

NOMENCLATURE

$\boldsymbol{a}$	acceleration of the casing $[m/s^2]$	$\boldsymbol{K_{ij}}$	stiffness coefficients $[N/m]$
$\boldsymbol{e}$	effective clearance $[m]$	$\boldsymbol{L}$	seal axial length $[m]$
$\boldsymbol{f_{ext}}$	applied force $[N]$	$\boldsymbol{M_{stator}}$	stator mass $[kg]$
$\boldsymbol{f_{fluid}}$	fluid-flow induced excitation force $[N]$	$\boldsymbol{P_d}$	downstream pressure $[Pa]$
$\boldsymbol{f_r}$	radial component of the seal reaction force $[N]$	$\boldsymbol{P_u}$	upstream pressure $[Pa]$
$\boldsymbol{f_\theta}$	tangential component of the seal reaction force $[N]$	$\mathbf{Q}$	flow coefficient $[\mathrm{K\,s^2/m^2}]$
$\boldsymbol{j}$	imaginary unit $(\sqrt{-1})$	$\boldsymbol{X(\omega), Y(\omega)}$	Fourier transform of $\delta x, \delta y$ $[m]$
$\dot{\boldsymbol{m}}$	mass flow rate $[kg/s]$	$\boldsymbol{\delta x, \delta y}$	displacement of stator with respect to the shaft $[m]$
$\boldsymbol{A}$	Fourier transform of a $[m/s^2]$	$\boldsymbol{\omega}$	angular frequency $(2\pi f)$ $[rad/s]$
$\boldsymbol{C_{ij}}$	damping coefficients $[Ns/m]$	$()^{\boldsymbol{i}}$	response ( ) due to excitation in the i direction

$\boldsymbol{D}$	seal diameter $[m]$	$(\ddot{})$	second time derivative $(d^2()/dt^2)$
$\boldsymbol{F_{ext}}$	Fourier transform of the applied force $[N]$	$(\dot{})$	time derivative $(d()/dt)$
$\boldsymbol{H_{ij}}$	frequency response functions (impedances) $[M/m]$		

INTRODUCTION

Gas turbines are designed to maximise work output and efficiency. Sealing technologies that minimise, and control, the leakage between rotating and stationary components are key to achieving these goals. The challenge for engine designers is therefore to minimise seal leakage, while at the same time preventing rubs occurring throughout a range of operational transients. Labyrinth seals are the most frequently employed non-contacting seals in turbomachinery. They present a relative low cost and long life solution with no restriction in speed, nor in pressure. However, labyrinth seals offer no compliance and therefore suffer from rubs during operation; labyrinth seal clearances increase with wear and, hence, suffer from diminishing performance. Compliant seals offer clear performance gains over labyrinth seals, although this promise is not without drawbacks.

Brush seals demonstrate performance improvements compared to labyrinth seals (Ferguson (1988)). Their leakage characteristics and seal depth are reduced, leading to increased overall thermal efficiency and decreased machine weight. Rotor misalignments (or indeed, rotor excursions during operation) have a smaller impact on brush seals as the bristles can flex to comply with the relative movement between the shaft and the machine casing. The main drawbacks of brush seals are their inability to withstand large pressure differentials and that bristle wear limits their life.

Leaf seals (Jahn et al. (2008)), shoed brush seals (Delgado et al. (2005)) and finger seals (Proctor et al. (2004)) are concepts developed to offer enhanced performance compared to brush seals. These seals are characterised as being *in contact* with the shaft at low rotating speeds and *lifting away* as the leakage mass-flow increases and creates a hydrodynamic film underneath the seal.

Further still, the latest turbomachinery sealing solutions are referred to as *non-contacting adaptive seals*, designed to avoid rubbing at all operating conditions. A relatively large clearance between the rotor and the stator exists during the start-up and shut-down phase of operation, when rotor and stator misalignments are the largest. As the pressure upstream of the seal increases, the sealing elements close down towards the shaft and the clearance decreases. An example of this type of seal is the Film Riding Pressure Actuated Leaf Seal (FRPALS) introduced by Grondahl and Dudley (2010).

This paper focuses on the design of a novel test facility for the experimental characterisation of shaft seals for turbomachinery. The rig is capable of assessing the leakage performance of shaft seals, subject to dynamic clearance variation between the rotor and stator. Measurements of force, acceleration and displacement allow for the rotordynamic characterisation of the seal to be determined. The first experimental campaign focusses on the performance of a labyrinth seal.

Literature Review: Labyrinth Seals

Labyrinth seals are known to create instabilities in compressors and turbines. Several studies have been carried out in order to determine the rotordynamic behaviour of this type of seal. Childs (1993) summarised the research into labyrinth seals to date. He concluded that, for seals with five or more cavities, the direct stiffness coefficient is negative and becomes increasingly negative as the number of cavities or running speed increases. The cross-coupled stiffness was shown to increase with the number of cavities, the inlet tangential velocity and the density within the seal. Finally, the direct damping coefficient is small in comparison, however plays an important role in the stability of the seals, counteracting the destabilising effect of the cross coupled stiffness.

Pelletti & Childs (1991) tested short labyrinth seals (L/D = 1/6) at rotor surface speeds of up to 127 m/s, upstream pressures of 30 bar and pressure ratios (P_d / P_u) ranging between 0.4 and 0.67. They found that decreasing the pressure ratio and increasing the rotational speed had a stabilising effect on the seal, whereas increasing pre-swirl at seal inlet and the seal clearance were destabilising.

Picardo and Childs (2005) investigated a labyrinth seal with 19 cavities and an *L*/*D* ratio of 3/4 at an upstream pressure of 70 bar and rotor surface speeds up to 243 m/s. They concluded that for small eccentricities between the rotor and the stator, the cross-coupled stiffness coefficients were equal in magnitude, but of opposite sign. In addition, the rotordynamic coefficients were found to be frequency independent up to a frequency of 150 Hz. More recently, Arthur and Childs (2015) compared the performance of a tooth-on-rotor (TOR) and a tooth-on-stator (TOS) labyrinth seal at the same experimental conditions. TOR seals were found to be more stable than TOS throughout the whole range of rotational speeds tested.

Rotordynamics of Annular Gas Seals

A linear model (Eq. (1)) is used to simulate the forces that arise due to changes in the pressure of the fluid film between the rotor and the seal. Figure 1 illustrates how the seal reaction forces are modelled by a spring-damper system.

$$-\begin{bmatrix} f_{fluid_x} \\ f_{fluid_y} \end{bmatrix} = \begin{bmatrix} K_{xx} & K_{xy} \\ K_{yx} & K_{yy} \end{bmatrix} \begin{bmatrix} \delta x \\ \delta y \end{bmatrix} + \begin{bmatrix} C_{xx} & C_{xy} \\ C_{yx} & C_{yy} \end{bmatrix} \begin{bmatrix} \dot{\delta x} \\ \dot{\delta y} \end{bmatrix} + \begin{bmatrix} M_{xx} & M_{xy} \\ M_{yx} & M_{yy} \end{bmatrix} \begin{bmatrix} \ddot{\delta x} \\ \ddot{\delta y} \end{bmatrix} \quad \textbf{(1)}$$

To understand the physical meaning of the rotordynamic coefficients, consider the whirling rotor of Figure 2, with rotational speed, ω, a precession with a forward orbit of amplitude, *A*, and rotational velocity, Ω. The seal forces in Eq. (1), reacting on the rotor and projected in the radial and tangential directions, are expressed in Eq. (2). Positive values of f_r and f_θ are *destabilising* for the rotor (moving it away from the seal centre), whereas negative values of these forces have a *stabilising* effect. Radial forces are typically small in labyrinth seals (Childs and Vance (1997)). The tangential component of the seal reaction force has a greater impact than the radial component on the stability of the seal. From Eq. (2), in order to have a stable system, the factor ($\Omega \cdot C - k$) has to be maximised; this is achieved by increasing the value of *C* or reducing *k*.

$$\begin{aligned} f_r &= -(K + \Omega \cdot c) \cdot A \\ f_\theta &= (k - \Omega \cdot C) \cdot A \end{aligned} \quad \textbf{(2)}$$

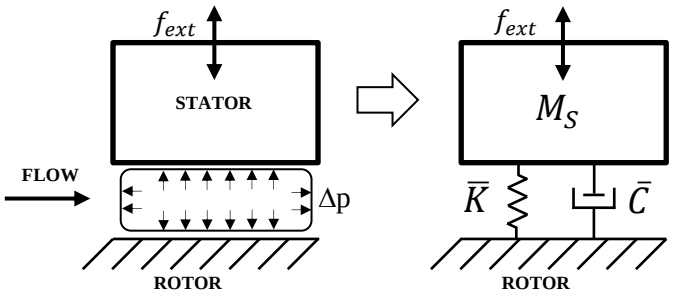

Figure 1: Model of the seal reaction forces as a spring-damper system. The frame of reference is fixed to the rotor.

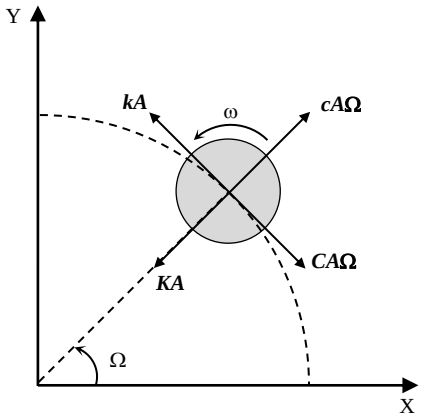

Figure 2: Schematic of the seal reaction forces on a whirling rotor. Adapted from Arthur and Childs (2015)

TEST RIG

Overview

Figure 3 shows a CAD representation of the new test facility; Figure 4 shows a cross-section view of the test section. The test section and the electric motor are located on top of a cast iron bedplate. A frame raises the bedplate from floor level and allows an electromagnetic shaker to be arranged underneath the test section. Compressed air at ambient conditions is supplied to a radial diffuser through a 50 mm diameter pipe. Once diffused, the air is split into 14 pipes, each of 19 mm diameter, before emerging into a small cavity, immediately upstream of the test section. Measurements of the static pressure in each supply pipe, and in the upstream cavity, indicate axisymmetric flow into the

test section; a maximum difference of 0.2% of the mean pressure was measured at all circumferential positions. A maximum pressure ratio of 3.5 bar across the test seal can be achieved in the rig.

In order to measure the rotordynamic coefficients of the test seal, a vibration test is performed. Contrary to the real engine scenario, where the rotor translates relative to the seal, the test facility has been designed so that the casing is shaken around the fixed rotor.

The rotor features a shaft and rotor disc, machined as one piece from forged EN40B nitrided, case-hardened, steel. The rotor is rigidly supported by grease lubricated bearings and the rotor disc, with a diameter of 254 mm and an axial length of 80 mm, overhangs the bearing block in a cantilever arrangement. A 15 kW variable-speed AC motor drives the shaft through a 3:1 ratio pulley system, up to a maximum rotational speed of 15,000 rpm; the maximum rotor surface velocity is 200 m/s.

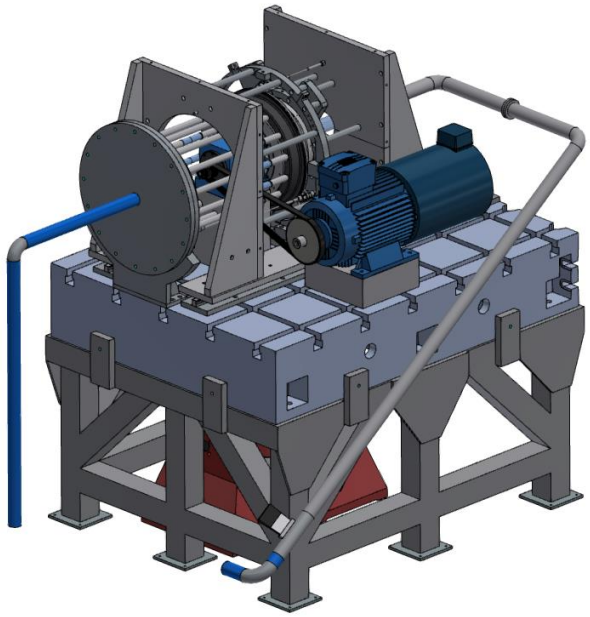

Figure 3: CAD representation of the test rig.

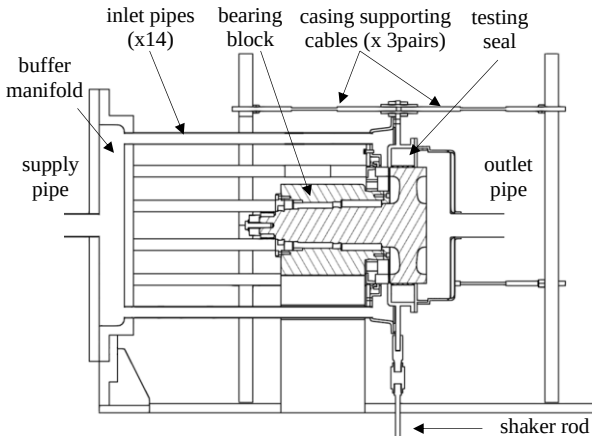

Figure 4: Cross section view of the test section.

The test seal is mounted in a casing that surrounds the rotor, containing the pressurised air in an annular test section; the leakage flow emerges into a collection system downstream of the seal. Three pairs of pre-tensioned cables support the casing, allowing for the stator assembly to be shaken and preventing out-of-plane movement between the seal and the rotor. A drive rod connects the casing to an electromagnetic shaker, designed according to the guidelines of Harris and Bush (2015).

The electromagnetic shaker is capable of exciting the stator in the vertical plane, with a maximum force of 3000 N and a maximum frequency of 4000 Hz. The magnitude of the force applied to the seal is measured by a load cell, installed in line with the drive rod. Additionally, the acceleration of the casing and the relative position between the casing and the rotor are measured by an accelerometer and an eddy current probe, respectively, in both the direction of shaking and the lateral plane. Two horizontal stiffeners are mounted in the lateral plane, restricting the movement of the casing in this direction. The reaction force of the casing against these stiffeners is measured with a further load cell, installed in line with the stiffeners.

The pressurised air supplied to the test section can flow along three different paths, shown in Figure 5, labelled as the *test seal*, *contact seal* and *secondary labyrinth seal*. The contact seal consists of a flexible rubber lip, located on the outer diameter of the bearing block. The flexibility of the rubber allows the casing to be translated. The secondary labyrinth seal is used to limit flow into the upstream cavity and also to reduce the axial thrust load on the rotor (required to maximise bearing life).

The leakage flow discharges into a carbon-fibre collection system before exiting the rig through an 80 mm pipe. Flow straighteners are mounted in the exit pipe to suppress the swirl of the flow introduced by the rotor, before the mass flow is measured by a Bronkhorst F-106CI thermal mass flow meter. If required, tests can be performed without the downstream collector in order to obtain visual access to the seal.

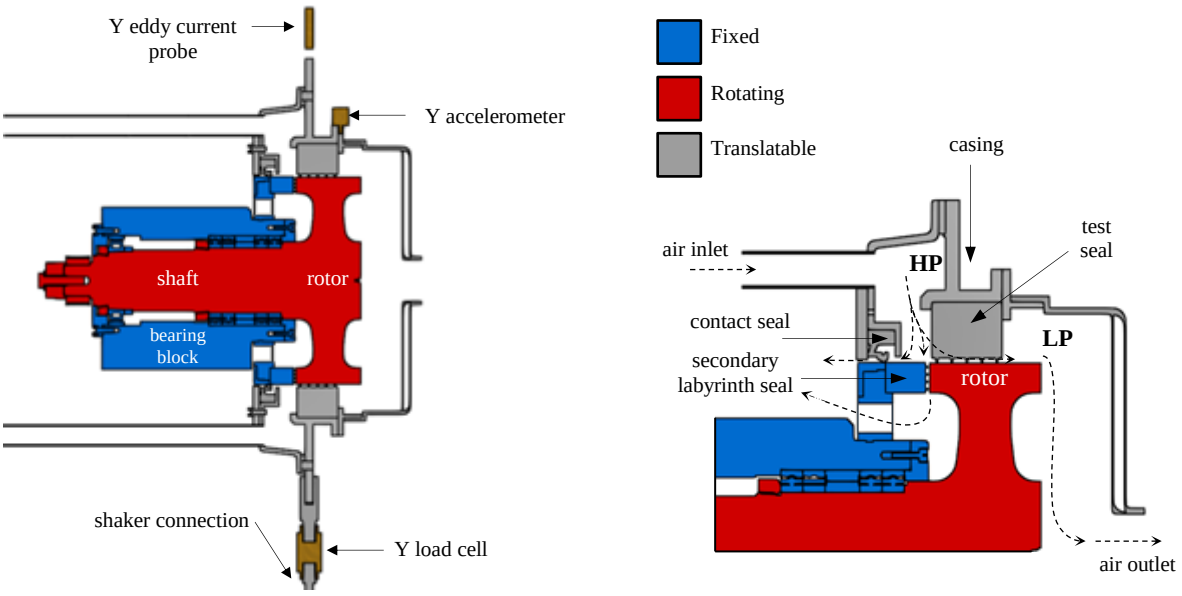

Figure 5: Close-up view of the test section: (a) details of instrumentation for rotordynamic coefficients and (b) flow paths in the test section

Data Acquisition

A National Instruments device with an analogue to digital converter of 16 bits is used to acquire the data. The signals used to calculate the rotordynamic coefficients (load cell, accelerometers and eddy current probe) are acquired simultaneously so that they have the same time reference. The input signals are filtered with analogue filters before being converted to digital to avoid aliasing problems. The cut-off frequency of the filters is 1250 Hz, well above 250 Hz (the maximum rotating frequency). A sampling frequency of 8,192 (2^{13}) Hz is used.

The shaker signal is controlled to fit a given displacement of the casing. The input signal to the shaker is a chirp signal that linearly varies the frequency from 10 to 250 Hz in 10 seconds. One experiment consists of one repetition of the input waveform. Five experiments are performed and the data averaged to account for variability.

LABYRINTH SEAL TEST

The geometry and dimensions of the labyrinth seal under investigation are shown below in Figure 6 and Table 1.

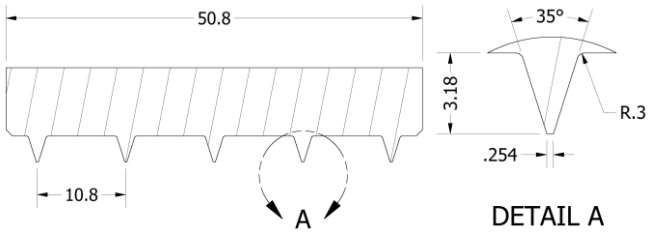

Figure 6: Schematic of the labyrinth seal under investigation.

Seal Diameter	254.28 mm
Seal Clearance	0.28 mm
No. of Cavities	4
Length/Diameter (*L/D*)	1/5
Cavity Width	10.8 mm
Cavity Height	3.18 mm
Tooth Thickness	0.25 mm

Table 1: Labyrinth seal dimensions.

Baseline Test

In order to isolate the reaction forces of the seal, the effect of the pre-tensioned wires supporting the casing and the contact rubber seal has to be measured and removed from the overall results of the vibration test. This is achieved by conducting a second shaking test in the absence of both flow and

rotation. The second test is referred to as baseline test and it is performed with exactly the same experimental setup. The effect of the secondary labyrinth seal on the rotordynamic coefficients is assumed to be negligible as the flow passing though this seal is parallel to the plane of shaking.

ROTORDYNAMIC COEFFICIENTS

Identification Methodology

The method developed by Rouvas and Childs (1993) is used. Newton's second law applied to the stator reads:

$$\sum \vec{f} = \vec{f}_{fluid} + \vec{f}_{ext} = \boldsymbol{M_{stator}} \cdot \vec{a} \tag{3}$$

where $\vec{f}_{ext}$ is the external force applied with the shaker, M_{stator} is the mass of the stator and $\vec{a}$ is the measured acceleration of the stator. The linear model for the forces generated by the fluid film between the rotor and the seal (f_{fluid_x}, f_{fluid_y}) of Eq. (1) is combined with Eq. (3) to give the following expression:

$$\begin{bmatrix} f_{ext_x} - M_{stator} \cdot a_x \\ f_{ext_y} - M_{stator} \cdot a_y \end{bmatrix} = \begin{bmatrix} K_{xx} & K_{xy} \\ K_{yx} & K_{yy} \end{bmatrix} \begin{bmatrix} \delta x \\ \delta y \end{bmatrix} + \begin{bmatrix} C_{xx} & C_{xy} \\ C_{yx} & C_{yy} \end{bmatrix} \begin{bmatrix} \dot{\delta x} \\ \dot{\delta y} \end{bmatrix} + \begin{bmatrix} M_{xx} & M_{xy} \\ M_{yx} & M_{yy} \end{bmatrix} \begin{bmatrix} \ddot{\delta x} \\ \ddot{\delta y} \end{bmatrix} \tag{4}$$

Note that, contrarily to what happens in a real engine, the absolute frame of reference is fixed to the rotor and the stator moves relative to it. This is depicted in Figure 1, which is a schematic representation of Eq. (4).

Assuming that the force applied with the shaker and the displacement components of the stator are sinusoidal functions as depicted in Eq. (5), transformation of Eq. (4) to the frequency domain results in Eq. (6):

$$\vec{f}_{ext} = \vec{A} \cdot cos\omega t;\ \overrightarrow{\delta x} = \vec{B} cos\omega t \tag{5}$$

$$\begin{bmatrix} F_{ext_x} - M_{stator} \cdot A_x \\ F_{ext_y} - M_{stator} \cdot A_y \end{bmatrix} = \begin{bmatrix} H_{xx} & H_{xy} \\ H_{yx} & H_{yy} \end{bmatrix} \begin{bmatrix} X \\ Y \end{bmatrix} \tag{6}$$

where F and A are the Fourier transforms of the applied force and the measured acceleration of the stator, respectively. In the same manner, X and Y are the direct Fourier transforms of the casing displacement measured in the time domain.

To completely determine the four components of H_{ij}, two separate excitations must be applied to the bearing, to yield independent sets of Eq. (6). This is done by sequentially exciting the seal in the X and Y directions, while holding the external force in the other direction equal to zero. However in this case it is assumed that $H_{yy} = H_{xx}; H_{yx} = -H_{xy}$ therefore only one excitation is needed to calculate the rotordynamic coefficients of the seal.

$$\begin{bmatrix} {F^x}_{ext_x} - M_{stator} \cdot {A^x}_x & {F^y}_{ext_x} - M_{stator} \cdot {A^y}_x \\ {F^x}_{ext_y} - M_{stator} \cdot {A^x}_y & {F^y}_{ext_y} - M_{stator} \cdot {A^y}_y \end{bmatrix} = \begin{bmatrix} H_{xx} & H_{xy} \\ H_{yx} & H_{yy} \end{bmatrix} \begin{bmatrix} X^x & X^y \\ Y^x & Y^y \end{bmatrix} \tag{7}$$
$$\equiv [A = H \cdot B]$$

H is obtained by solving Eq. (7):

$$H = A \cdot B^{-1} \tag{8}$$

Finally, each term of the matrix H_{ij}, is a function of the frequency and of the rotordynamic coefficients:

$$H_{ij} = K_{ij} + j\omega C_{ij} - \omega^2 M_{ij} \tag{9}$$

If the real part of the complex stiffness, $Re(H_{ij})$ is fitted with a second order polynomial, the zero-frequency intercept corresponds to the stiffness coefficient of the seal, and the second order coefficient to the added mass of the seal. The damping is determined by the first order coefficient

(slope) of a linear curve fit passing through the origin of the imaginary part of the complex stiffness, $Im(H_{ij})$.

Figure 7 shows the frequency response function of the complex stiffness *H* for data collected at 14,600 rpm and 2.9 bar pressure difference. The three sets of data in each figure show the process followed to obtain to the final rotordynamic coefficients. The dark line corresponds to the frequency response function of the casing assembly shaken between 0 and 160 Hz with flow and rotation. The light curve is the frequency response function of the casing in the absence of flow and rotation (baseline test). By subtracting these two results, the complex stiffness corresponding to the thin film created in between the rotor and the labyrinth seal is obtained. This resultant distribution is fitted with Eq. (9), as explained in the paragraph above.

In Figure 8 (a), the curves corresponding to the tests with flow and rotation, and the baseline test have the same curvature. This indicates that, for both experiments, the same mass has been shaken and, when one of the plots is subtracted from the other, the second order coefficient of the resulting curve is zero. Therefore, the real part of the direct complex stiffness corresponding to the fluid thin film of the labyrinth seal is invariant with frequency, meaning that the film does not have any added inertial effect.

The same is expected for the cross-coupled complex stiffness shown in Figure 8 (b), however the curve corresponding to the thin film has a polynomial fit with a second order coefficient different to zero.

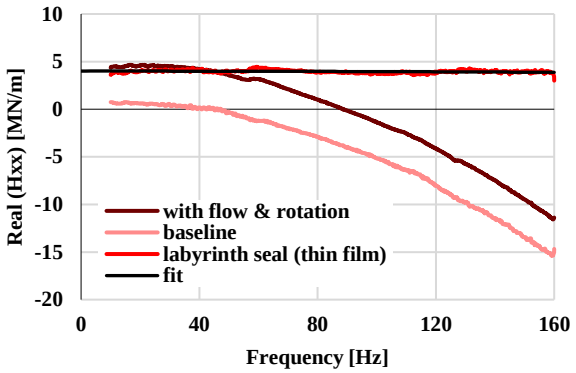

(a) Real part of the direct complex stiffness Re(H_{xx}) and second order curve fit

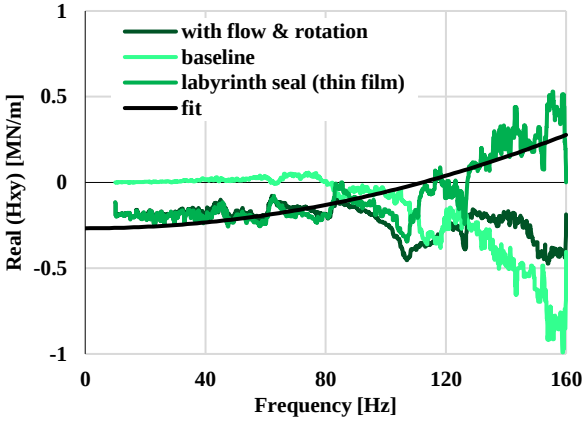

(b) Real part of the direct complex stiffness Re(H_{xy}) and second order curve fit

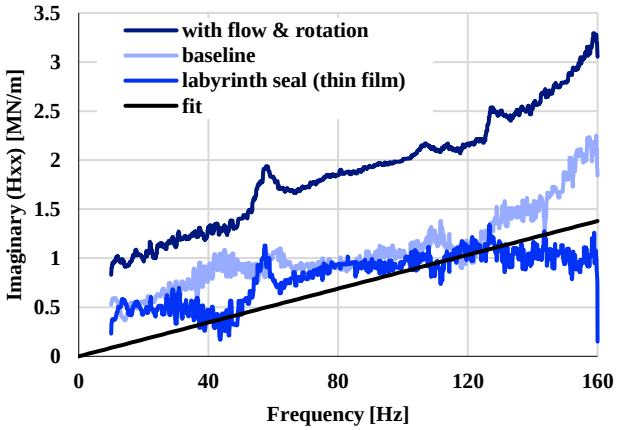

(c) Imaginary part of the direct complex stiffness $Im(H_{xx})$ and linear fit.

Figure 7: Complex stiffness against frequency for the baseline test, the test with flow and rotation and the resulting thin film. All experiments conducted at a rotational speed of 14,600 rpm and a pressure difference of 2.9 bar.

RESULTS

Effective Clearance

The effective clearance is defined as the clearance of an annular restriction of the same diameter as the tested seal required to pass the measured leakage isentropically. Typically this parameter is used to compare the leakage performance of seals of different type and geometry as it accounts for the test conditions and the dimensions of the tested seals. Eqs. (10) and (11) are used to calculate the effective clearance.

$$e = \frac{\dot{m}\sqrt{T}}{\pi p_u D Q} \tag{10}$$

$$Q = \begin{cases} \sqrt{\dfrac{2\gamma}{R(\gamma-1)}\left(\left(\dfrac{p_u}{p_d}\right)^{\frac{-2}{\gamma}} - \left(\dfrac{p_u}{p_d}\right)^{-\left(\frac{\gamma+1}{\gamma}\right)}\right)} & for\ \left(\dfrac{p_u}{p_d}\right) < \left(\dfrac{2}{\gamma+1}\right)^{-\left(\frac{\gamma}{\gamma-1}\right)} \\ \sqrt{\dfrac{\gamma}{R}\left(\dfrac{2}{\gamma+1}\right)^{\frac{\gamma+1}{\gamma-1}}} & for\ \left(\dfrac{p_u}{p_d}\right) > \left(\dfrac{2}{\gamma+1}\right)^{-\left(\frac{\gamma}{\gamma-1}\right)} \end{cases} \tag{11}$$

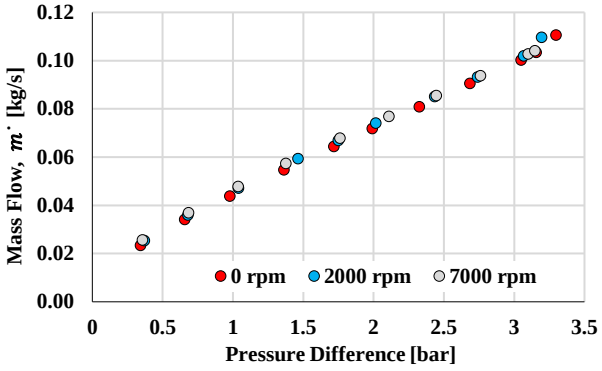

Figure 8: Variation of mass flow rate with pressure difference for three rotational speeds.

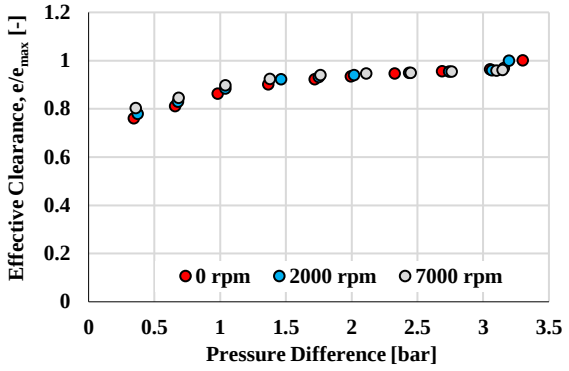

Figure 9: Variation of effective clearance with pressure difference for three rotational speeds.

The leakage mass flow rate of the labyrinth seal at three rotational speeds is plotted against pressure difference in Figure 8. The data shows the leakage mass flow rate is independent of rotational speed across the range tested. The effective clearance corresponding to the measured mass flow rate is shown in Figure 9. The data is presented in dimensionless form by normalising against the maximum effective clearance found during the experiments.

Rotordynamic Coefficients

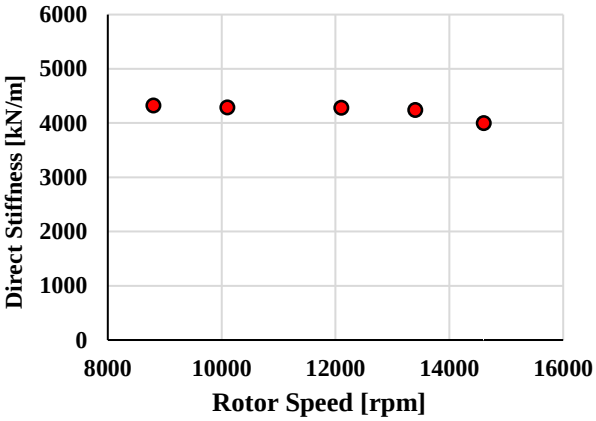

Figure 10: Variation of direct stiffness with rotational speed for a pressure ratio of 0.26.

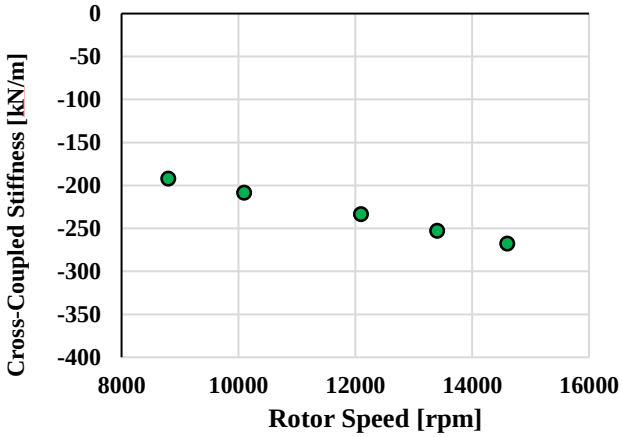

Figure 11: Variation of cross-coupled stiffness with rotational speed for a pressure ratio of 0.26.

The rotordynamic coefficients of the labyrinth seal described above are presented in this section. The tests were conducted at an upstream pressure of 3.9 bar and a pressure ratio, P_d/P_u, of 0.26 for five different rotational speeds: 8,800, 10,100, 12,100, 13,400 and 14,600 rpm.

Figure 10 shows the direct stiffness coefficient is invariant with rotational speed. This is obtained by extrapolation of the fit in Figure 8 (a) to the point of intersection with the y-axis at a frequency of zero. The cross-coupled stiffness is shown to increase in magnitude with rotational speed in Figure 12. Once again, this is obtained by extrapolation of the fit in Figure 8 (b). This increase implies a drop of stability with rotational speed, which can be explained by the fact that the air acquires a larger tangential component as the rotational speed increases when passing through the cavities.

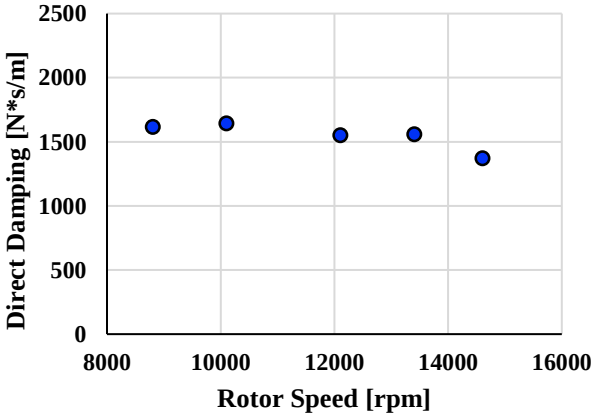

Figure 12: Variation of direct damping with rotational speed for a pressure ratio of 0.26.

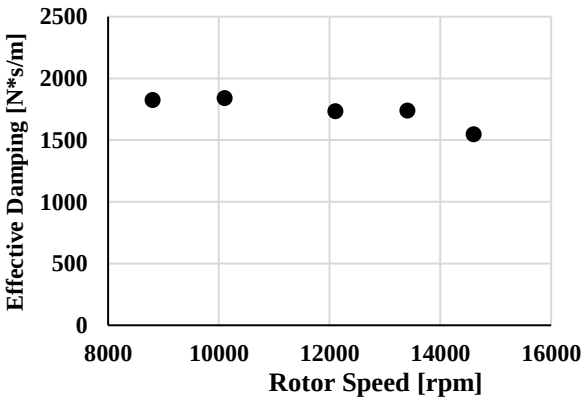

Figure 13: Variation of effective damping with rotational speed for a pressure ratio of 0.26.

The direct damping coefficient of the seal is shown to slightly decrease with rotational speed in Figure 12. This coefficient is determined by the gradient of the line of best fit in Figure 8 (c).

Effective damping takes into account the combined effect of the cross-coupled stiffness and the direct damping, and therefore is the best parameter to assess the stability of annular gas seals (Childs and Vance (1997)). It is proportional to the tangential reaction force of the seal on the rotor (Eq. (2)). It is calculated as $C_{eff} = C - k/\omega$, where ω is the rotational speed in rad/s. In order to increase seal stability the effective damping has to be maximised. Figure 13 shows the effective damping of the tested labyrinth seal for at a pressure difference of 2.9 bar and five rotational speeds.

CONCLUSIONS

A new high-speed rotating test facility capable of accommodating different turbomachinery shaft seals has been introduced. The rig was specifically designed for the assessment of leakage performance and determination of rotordynamic coefficients for novel non-contacting adaptive seals. Measurements of rotordynamics coefficients for rotational speeds of up to 15,000 rpm and pressure differences of up to 3.5 bar were demonstrated. A short (L/D = 1/5) labyrinth seal with four cavities and a nominal clearance of 0.28 mm was chosen as the example test case.

The variation of leakage mass flow rate with pressure difference for the labyrinth seal was shown to be independent of rotational speed across the range tested. The rotordynamic measurements showed that the direct stiffness was invariant with rotational speed. In contrast, the cross-coupled stiffness was shown to increase in magnitude whereas the direct damping coefficient decreased as the rotational speed increased.

FUTURE WORK

In the future the rig will be used to test non-contacting adaptive seals such as the FRPALS, introduced by Grondahl and Dudley (2010). The FRPALS incorporates two sets of axially displaced seal leaves with attached segmented runners. The presence of a differential pressure acting across the seal encourages the leaves and runners to displace in the radial direction until balanced by hydrostatic lift at a small clearance. The seal design provides a sufficient radial range of operation to follow the rotor during transients whilst mitigating against the interference problems of friction, heat and wear. Figure 15 shows the test arrangement with the FRPALS installed in the rig.

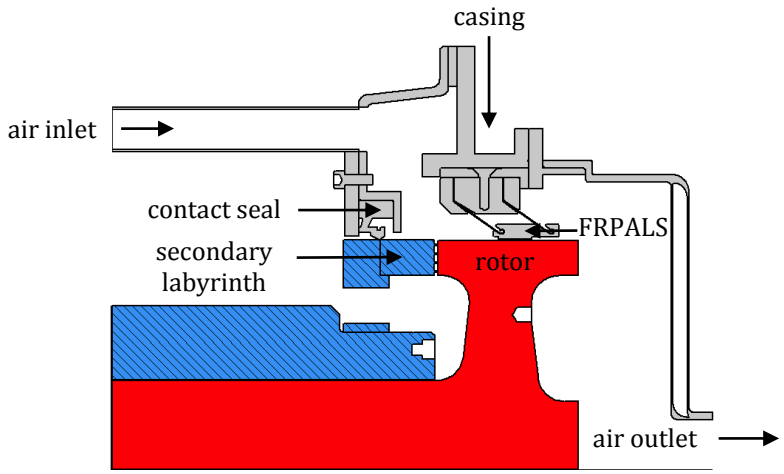

Figure 14: Test setup showing the FRPALS installed.

REFERENCES

Arthur, S. P. and Childs, D. W., 2015, "Measured Rotordynamic and Leakage Characteristics of a Tooth-on-Rotor Labyrinth Seal with Comparisons to a Tooth-on-Stator Labyrinth Seal and Predictions", ASME Paper GT2015-43242.

Childs, D., 1993, "Turbomachinery Rotordynamics: Phenomena, Modeling, and Analysis". John Wiley & Sons.

Childs, D. W. and Vance, J. M., 1997, "Annular Gas Seals and Rotordynamics of Compressors and Turbines", Proceedings of the 26th Turbomachinery Symposium, Texas A&M University. Turbomachinery Laboratories.

Delgado, A., San Andrés, L. and Justak, J. F., 2005, "Measurements of Leakage, Structural Stiffness and Energy Dissipation Parameters in a Shoed Brush Seal", Sealing Technology, 12, pp. 7-10.

Ferguson, J., 1988, "Brushes as High Performance Gas Turbine Seals", ASME Paper 88-GT-182.

Grondahl, C. M. and Dudley, J. C., 2010, "Film Riding Leaf Seals for Improved Shaft Sealing", ASME Paper GT2010-23629.

Harris, D. M. and Bush, J. W., 2015, "Generating Uniaxial Vibration With an Electrodynamic Shaker and External Air Bearing", Journal of Sound and Vibration, 334, pp. 255-269.

Jahn, I. H., Owen, A. K., Franceschini, G. and Gillespie, D., 2008, "Experimental Characterisation of the Stiffness and Leakage of a Prototype Leaf Seal for Turbine Applications", ASME Paper GT2008-51206.

Picardo, A. and Childs, D. W., 2005, "Rotordynamic Coefficients for a Tooth-on-Stator Labyrinth Seal at 70 Bar Supply Pressures: Measurements Versus Theory and Comparisons to a Hole-Pattern Stator Seal", ASME J. Eng. Gas Turb. Power, 127(4), pp. 843-855.

Proctor, M. P., Kumar, A. and Delgado, I. R., 2004, "High-Speed, High-Temperature Finger Seal Test Results", J. Propul. Power, 20(2), pp. 312-318.

Rouvas, C. and Childs, D. W., 1993. "A Parameter Identification Method for the Rotordynamic Coefficients of a High Reynolds Number Hydrostatic Bearing", Journal of Vibration and Acoustics, 115(3), pp. 264-270.